

www.acsnano.org

# Correlative Super-Resolution and Atomic Force Microscopy of DNA Nanostructures and Characterization of Addressable Site Defects

Christopher M. Green,\* William L. Hughes, Elton Graugnard, and Wan Kuang\*



Cite This: https://doi.org/10.1021/acsnano.1c01976



**Read Online** 

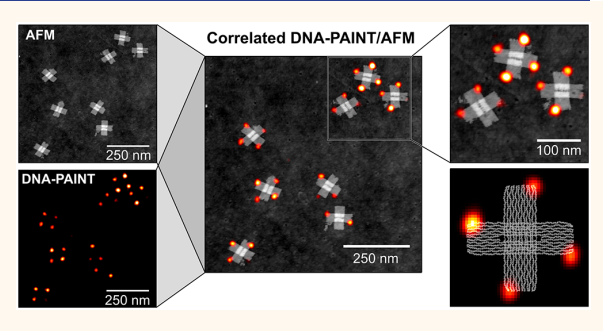
**ACCESS** I

Metrics & More

Article Recommendations

s Supporting Information

ABSTRACT: To bring real-world applications of DNA nanostructures to fruition, advanced microscopy techniques are needed to shed light on factors limiting the availability of addressable sites. Correlative microscopy, where two or more microscopies are combined to characterize the same sample, is an approach to overcome the limitations of individual techniques, yet it has seen limited use for DNA nanotechnology. We have developed an accessible strategy for high resolution, correlative DNA-based points accumulation for imaging in nanoscale topography (DNA-PAINT) super-resolution and atomic force microscopy (AFM) of DNA nanostructures, enabled by a simple and robust method to selectively bind



DNA origami to cover glass. Using this technique, we examined addressable "docking" sites on DNA origami to distinguish between two defect scenarios—structurally incorporated but inactive docking sites, and unincorporated docking sites. We found that over 75% of defective docking sites were incorporated but inactive, suggesting unincorporated strands played a minor role in limiting the availability of addressable sites. We further explored the effects of strand purification, UV irradiation, and photooxidation on availability, providing insight on potential sources of defects and pathways toward improving the fidelity of DNA nanostructures.

KEYWORDS: DNA nanotechnology, correlative microscopy, DNA-PAINT, DNA origami, super-resolution, AFM, metrology, SRM

NA-directed self-assembly offers precise spatial control when arranging molecules and particles at the nanoscale. 1-4 The utility of DNA origami has been demonstrated through multiple applications, such as plasmonic and photonic devices, 6-16 localized chemical reaction networks for sensing and DNA computation, 15 lithographic masks for semiconductor devices, 25-30 and protein/enzyme-based biosensors. 16,17,20,21,31,32 Many of these applications rely on the inclusion of addressable sites, typically single-stranded (ss) DNA tethers, for postassembly modification. The availability of such sites on the origami is critical to the synthesis of functional structures. Despite significant improvements in the design and synthesis of DNA origami, 12,33-44 over 10% of addressable sites are consistently defective and adversely affect performance. While the source of inactive sites has been attributed to unincorporated staple strands,<sup>39</sup> defective tethers,<sup>8</sup> and steric hindrance of conjugated molecules, 8,10 a systematic study of the root cause has yet to be carried out.

The challenges of identifying and overcoming factors that limit the availability of addressable sites on DNA nanostruc-

tures are shared throughout the field, as anticipated applications of DNA nanotechnology, especially those in healthcare, will be subject to strict standards on product purity and function. 45–47 Such challenges are exacerbated by a lack of characterization techniques enabling direct and reliable defect metrology on the scale of single staple strands. Common high-resolution microscopies, such as atomic force microscopy (AFM) and electron microscopies, enable detailed topographic and structural characterization of DNA nanostructures, though additional information—such as the sequence, presence, and availability of addressable sites—is often inaccessible. Conversely, DNA-PAINT super-resolution microscopy (SRM) enables the direct characterization of addressable sites on

Received: March 6, 2021 Accepted: June 7, 2021



DNA origami,<sup>39,48–54</sup> though inactive sites are indicated by a lack of detection and do little to elucidate the cause of such inactivity. Considering their attributes and abilities, DNA-PAINT and AFM are particularly well suited for correlative microscopy, serving as enabling technologies toward determining the root cause of inactive sites on DNA nanostructures.

While certain super-resolution techniques have been combined with AFM,  $^{55}$  correlative DNA-PAINT and highresolution AFM (HR-AFM) imaging of DNA nanostructures has not been possible due to incompatible substrate requirements. Here, we introduce a simple and robust method to selectively bind DNA origami (and not short ssDNA imager strands) directly to cover glass, enabling correlative DNA-PAINT/AFM imaging with no loss in quality of the respective techniques. We employed high-resolution, correlative microscopy to characterize DNA origami cross-tiles, 59,60 achieving spatial correlation between optical and topographic images that surpassed the resolution of the DNA-PAINT images. Inactive sites (sites not detected in DNA-PAINT despite their intended inclusion as active sites) were identified in DNA-PAINT images and subsequently examined in AFM for structural defects consistent with unincorporated staple strands. The results, surprisingly, showed little correlation between inactive sites and unincorporated staple strands; on average, 97% of addressable strands were observed to be incorporated, and unincorporated strands accounted for less than 25% of inactive sites. These results suggest that strand incorporation might play a smaller role in limiting DNA origami addressability than previously reported,<sup>39</sup> warranting further work to identify other factors that limit addressability. Motivated by reports in the literature, 56,57 we briefly investigated the role of docking site truncations, sequence errors, and photoinduced damage by UV exposure and imaging on site availability. The results suggest that improvements in the availability of addressable sites are challenging but attainable, and further investigations of mechanisms that limit site availability are warranted. Overall, this work validates the utility of correlative DNA-PAINT/AFM microscopy for enhanced characterization of DNA nanostruc-

## **RESULTS AND DISCUSSION**

Cross-Compatible Substrate for Correlative Imaging. Correlative microscopies are often constrained by a lack of substrates and sample preparation techniques that are simultaneously compatible with two distinct characterization techniques. For example, light and electron microscopies are powerful and complementary tools for the study of biological specimens but have differing sample preparation requirements.<sup>58</sup> In the case of DNA-PAINT and HR-AFM, a crosscompatible substrate that combines transparency, favorable DNA origami adsorption, low affinity for ssDNA imager strands, and near atomic-level flatness was previously lacking. For DNA-PAINT, DNA origami are typically bound to cover glass by biotin-avidin binding between biotinylated DNA present in the origami and surface-bound, biotinylated proteins (commonly biotinylated bovine serum albumin-BSA-biotin). The surface-bound proteins also passivate the surface to diffusing imager strands during image acquisition, reducing background noise and thus increasing the achievable resolution of single molecule localization.<sup>48</sup> While protein-binding is ubiquitous for DNA-PAINT, protein-coated surfaces are too rough for HR-AFM imaging of DNA nanostructures.

As an alternative to protein binding and passivation, we explored methods to modify the surface of cover glass to enable direct adsorption and immobilization of DNA origami while simultaneously passivating the surface to diffusing imager strands. We found that strongly oxidizing cleaning techniques (e.g., radiofrequency (RF) plasma in low pressure air, piranha solution, and heated ultraviolet (UV) and ozone exposure) produced cover glass surfaces to which DNA origami adsorbed irreversibly in standard DNA origami tris-buffers with magnesium while displaying strong passivation to imager strand adsorption. Of the techniques explored, plasma cleaning was the most effective method to prepare cover glass for imaging, and the results presented herein pertain to substrates prepared by glow discharge plasma cleaning. While we do not attempt to elucidate the chemical composition of the surface postcleaning, it was observed that DNA origami adsorption does not occur in the absence of divalent cations and at pH less than 7. This behavior is similar to prior observations of DNA origami adsorption to piranha/HF-cleaned, thermally grown silica, for which it was postulated that pH-dependent adsorption resulted from the deprotonation of silanol groups generated during cleaning.2

For the work described here, methods can be found in the Materials and Methods section. Additional information can be found in Supporting Information A and B, including details on the design and synthesis of the DNA origami cross-tile (adapted from Aghebat et al.)<sup>59,60</sup> shown in Supporting Information (SI) Figure S1. The results of our preliminary experiments on plasma-processed cover glass substrates and a comparison to biotin—avidin binding are provided in SI Figures S2—S4. In short, our protocol for preparing cover glass for DNA-PAINT and AFM microscopy consisted of two stages:

- A two-step ultrasonic agitation in dilute surfactant solution (0.1% v/v of Liquinox in water) and deionized (DI) water to remove large particulates. Cover glass were fully dried after cleaning.
- (2) Plasma processing of cover glass by glow discharge plasma in low pressure air.

This simple protocol enabled high signal-to-noise (>10:1) fluorescent events in total internal reflection fluorescence (TIRF) images during DNA-PAINT, strong passivation of the surface to imager stands to minimize nonspecific binding, and low surface roughness for high resolution AFM topography. Figure 1 shows independent examples of DNA-PAINT and HR-AFM images of DNA origami cross-tiles on plasmacleaned cover glass in identical buffer conditions, demonstrating that the individual techniques can be performed without a loss in quality relative to typical operating conditions. Given the simplicity and efficacy of the technique, plasma-cleaned cover glass was found to be an ideal substrate for correlative DNA-PAINT and AFM microscopy, as well as a desirable alternative to traditional methods for standalone imaging.

Correlative DNA-PAINT/AFM Microscopy. With a cross-compatible substrate identified, the next challenge for correlative microscopy was image registration, reliably relocating and aligning a small imaging area on a transparent substrate (~0.05 mm per side) in two separate microscopes. As an accessible solution to image registration, cover glass were lightly inscribed prior to cleaning to create registration marks visible with an optical objective. Additionally, a custom cover glass substrate mount (SI Figure S2) was developed to enable

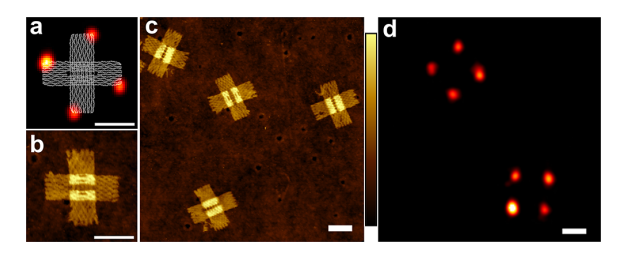


Figure 1. DNA-PAINT and AFM imaging of DNA origami on plasma-processed cover glass. (a) Atomistic model of the DNA origami cross-tile with DNA-PAINT image overlaid to indicate the position of docking sites. (b) HR-AFM height image of a DNA origami cross-tile on plasma-cleaned cover glass. The image was rotated to align with the model in (a). (c) HR-AFM height image and (d) DNA-PAINT image of DNA origami cross-tiles on processed cover glass. The full AFM image can be found in SI Figure S5. Scale bars, 50 nm. AFM height scale bar, 4 nm.

Exchange-PAINT imaging and nondestructive recovery of the substrate,  $^{50}$  though methods of substrate recovery from a traditional microscope slide and cover glass microchannel were also successfully employed. For correlative DNA-PAINT/AFM imaging of DNA origami cross-tiles, cross-tiles were deposited directly onto the surface of glow discharge-treated cover glass and incubated for 30 min. Buffer exchanges were performed after incubation and immediately prior to imaging. DNA-PAINT images of 55  $\times$  55  $\mu$ m<sup>2</sup> were acquired over 1 h on an

inverted Nikon Eclipse Ti microscope. After optical imaging, samples were rinsed with fresh buffer and transported for AFM imaging. Cover glass were recovered from the substrate mount and mounted on silicone pads or metal pucks for alignment and AFM imaging in buffer. Independent high-resolution and large area AFM images ( $2 \times 2 \mu \text{m}^2$  with  $1 \text{ nm}^2$  pixels and  $20 \times 20 \mu \text{m}^2$  with  $100 \text{ nm}^2$  pixels, respectively) were acquired to assess the quality of correlation between cross-tiles in DNA-PAINT and AFM images and to assess the stability of DNA origami during imaging. The experimental procedure is depicted in SI Figure S6, and representative results of correlative DNA-PAINT/AFM imaging of DNA origami at various scales are shown in Figure 2.

We found that origami were consistently well-correlated in DNA-PAINT/AFM after applying image postprocessing corrections for global image distortions, which result from aberrations of the individual techniques such as field curvature and thermal drift (SI Figures S7–10). To quantitatively assess the quality of correlation, two sets of correlated DNA-PAINT and AFM images were examined for differences in the relative positions of docking sites within the images. Two-dimensional dispersion was determined from the distribution of spatial deviations between individual sites in each image, depicted in Figure 3. For 286 independent docking sites, the mean spatial deviation ( $\sigma_{xy}$ ) was 5 ± 3 nm. The deviations were independent of position (Figure 3d,e), indicating that global distortions were well-corrected and unlikely to contribute significantly to spatial deviations. Rather, the

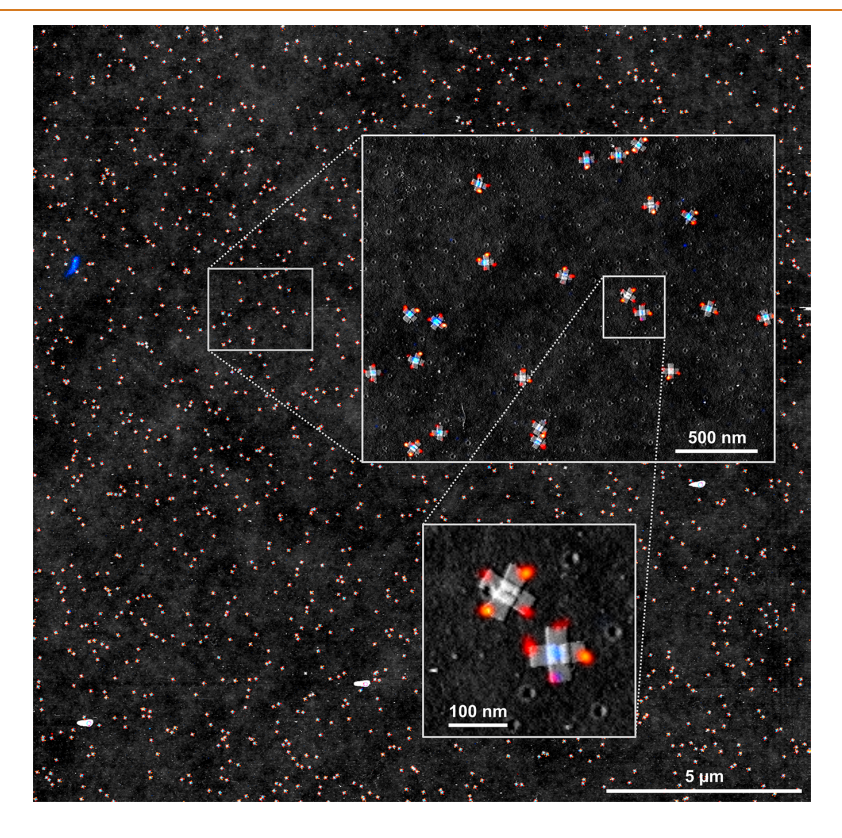


Figure 2. 20  $\mu$ m  $\times$  20  $\mu$ m correlative DNA-PAINT/AFM image of DNA origami cross-tiles. The large area AFM image was acquired with 10 nm pixel size, and the inset images were acquired with 2.5 nm pixel size. To enhance the contrast of features in AFM images, the height and amplitude error channels were superimposed.

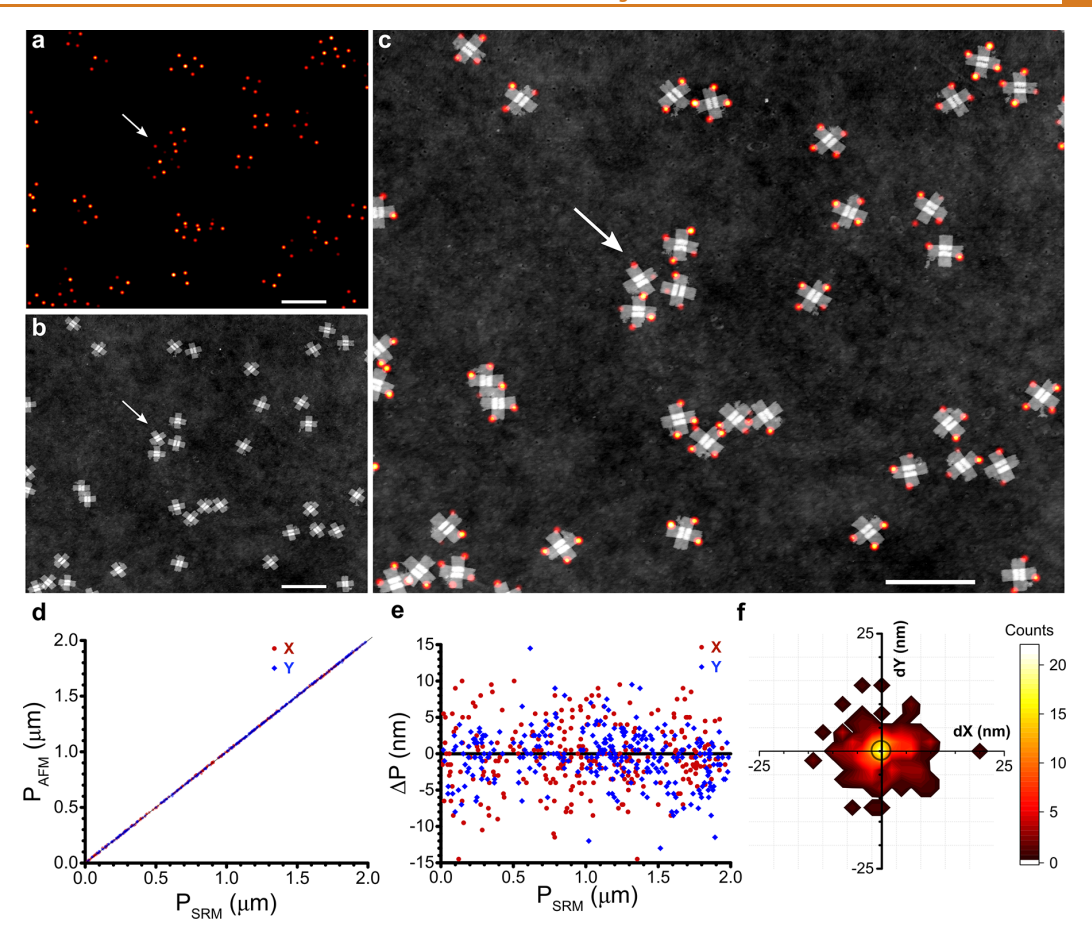


Figure 3. Quantifying spatial correlation of docking sites in DNA-PAINT and AFM images. (a) DNA-PAINT, (b) AFM, and (c) combined DNA-PAINT/SRM image of DNA origami cross-tiles. White arrows indicate a common feature within the images for visual aid. Scale bars, 250 nm. (d-f) Spatial correlation, dispersion, and 2D dispersion histogram, respectively, of 286 docking sites in correlated DNA-PAINT and AFM images (SI Figures S10 and 17).  $P_{AFM}$  and  $P_{SRM}$  represent the positions of corresponding docking sites in AFM and SRM images, respectively, with horizontal (X, red) and vertical (Y, blue) positions indicated.  $\Delta P$  represents the deviation in position of corresponding sites in DNA-PAINT and AFM. dX and dY represent the deviation between corresponding sites in the X and Y axes, respectively. The mean spatial deviation of individual sites was 5  $\pm$  3 nm, depicted by a black circle near the origin.

observed spatial deviations could be accounted for by uncertainty in single molecule localizations ( $\sigma_{loc}=6\pm2$  nm, SI Figure S10), further suggesting that adsorbed origami were completely immobile on the surface. These results demonstrate that optimal performance of the individual techniques could be maintained during correlative imaging with no observable movement of individual origami, enabling a 1:1 mapping of DNA-PAINT to AFM topography and validating correlative imaging for single-strand defect metrology.

**Defect Metrology.** With high-resolution correlative imaging, we sought to determine whether two docking site defect scenarios, previously described by Strauss et al., <sup>39</sup> could be distinguished: (1) incorporated but inactive sites: strands that are present in the origami but lack an active docking site, and (2) unincorporated sites: strands that are missing entirely from the origami. Prior to this work, it had not been possible to directly distinguish inactive sites from unincorporated sites due to the binary nature of DNA-PAINT, for which both scenarios result in a lack of detection. Conversely, HR-AFM enables the detection of unincorporated sites (SI Figure S11) but does not enable determination of whether an incorporated

site is active or inactive, providing a similarly binary characterization of docking sites. Through correlative DNA-PAINT/AFM microscopy, information attained with each technique can be leveraged simultaneously to distinguish between active, inactive, and unincorporated sites as depicted in Figure 4. Though it is not discussed in depth here, it should be noted that the quality of defect metrology with correlative microscopy is dependent on the fidelity of observations made with the individual techniques. For example, if DNA-PAINT imaging is performed with insufficient time to detect all available docking sites, many sites will falsely appear to be defective in DNA-PAINT without correlating to defects in AFM, resulting in a skewed distribution of observed defects. Several methods and experiments were thus employed to quantify performance and minimize the largest sources of uncertainty during defect characterization, namely the degree of image acquisition with DNA-PAINT and the probability of detecting unincorporated site defects with HR-AFM; these are discussed in detail in SI B3-B5 and depicted in Figures S11-S14. We also limited our studies to edge sites on the DNA origami cross-tile to ensure that unincorporated sites could be

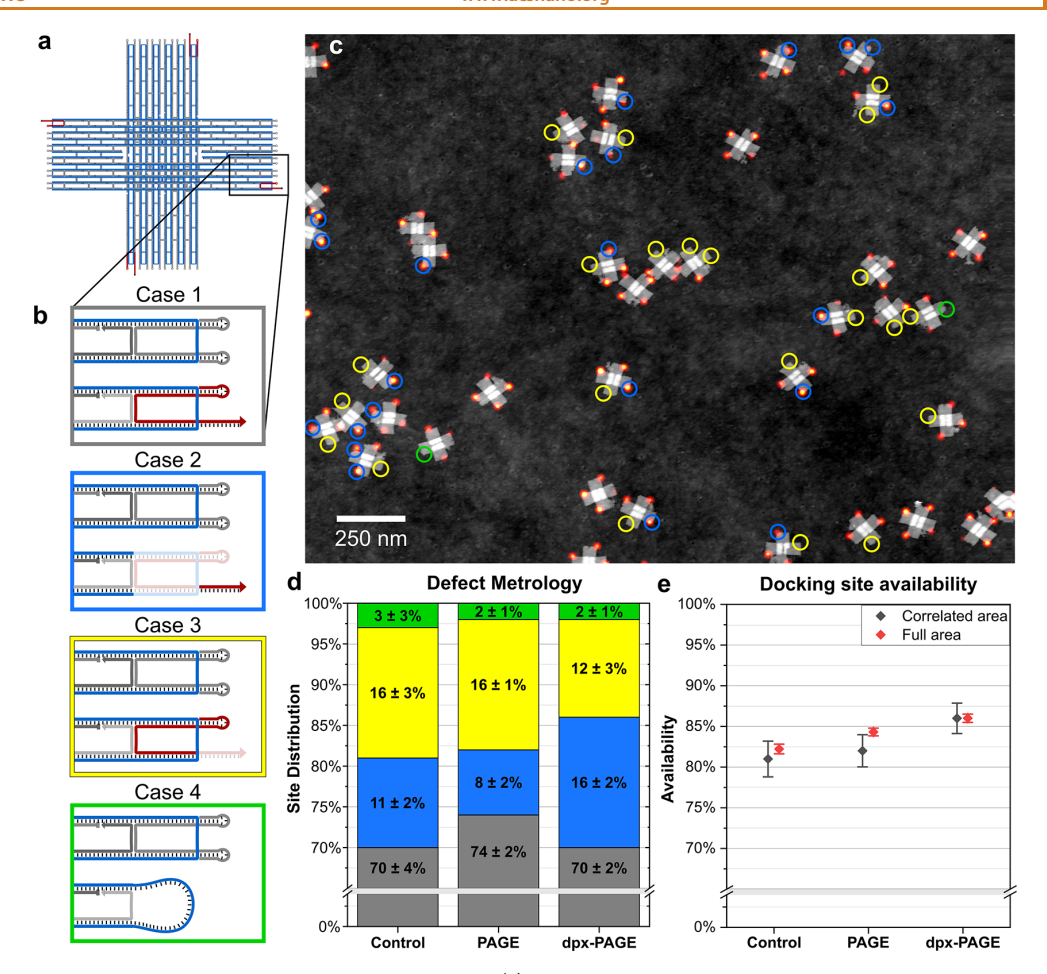


Figure 4. Correlation of defects in DNA-PAINT and AFM images. (a) Strand diagram of the DNA origami cross-tile depicting the positions of docking sites (red) at one corner of each arm. (b) Magnified strand diagrams depicting the four possible cases for docking sites classified by correlation of DNA-PAINT and AFM images. (c) Representative correlated DNA-PAINT/AFM image of cross-tiles; individual docking sites are marked as Case 2 (blue), Case 3 (yellow), or Case 4 (green). (d) Bar plot summarizing the results of defect metrology for cross-tiles containing unfiltered docking sites (Control, n = 319), PAGE-filtered docking sites (PAGE, n = 377), and duplexed, PAGE-filtered docking sites (dpx-PAGE, n = 344). Colored segments correspond to the cases in (b). Correlated images and the results of defect metrology for each sample can be found in SI Figures S15–17. (e) Plot of the docking site availability for each sample as determined by correlative metrology (gray, availability reported as Case 1 + Case 2) and automated classification of full area DNA-PAINT images (red).

reliably detected with AFM, though studies of internal sites are likely feasible with this technique. In short, the results demonstrated that (1) unincorporated strands were readily detectable in HR-AFM images, and (2) DNA-PAINT imaging approached 99% completion in 1 h for the conditions employed in correlative imaging, lending confidence to observations made from the combined techniques.

To classify and quantify strand defects on DNA origami and further shed light on mechanisms contributing to the perceived limits of site addressability, we performed a set of investigations into strand defects introduced during synthesis. To reduce the occurrence of strand defects potentially introduced during oligo synthesis, such as strand truncations and base substitutions, insertions, and deletions, docking site strands were filtered with polyacrylamide gel electrophoresis (PAGE) as ssDNA or as a duplex strand hybridized at the docking site domain prior to origami synthesis (SI A14–A16). The latter technique was employed with the goal of targeting defects that traditional PAGE filtration is insensitive to on

ssDNA—namely defects which do not alter the length of a strand—by selectively doubling the length of strands possessing an active docking site. All samples were additionally filtered by agarose gel electrophoresis (AGE) after origami synthesis.

Correlative DNA-PAINT/AFM microscopy was performed on each filtered sample and a control origami assembled with unfiltered strands, and corresponding images were postprocessed, aligned, and corrected for image aberrations. Individual cross-tiles were examined in AFM images for edge defects, indicated by a shortened tile edge which appears as an indentation in the corner of a tile arm or rounding of the corner (SI Figure S11). Similarly, cross-tiles were inspected in DNA-PAINT images for unresolved sites, then sites in corresponding images were correlated by position and combined to distinguish between the two types of defects described previously. The combined classifications for individual sites resulted in four distinct scenarios, referred to here as Cases 1–4 (Figure 4b). Sites at which no defects were

observed in DNA-PAINT and AFM are classified as Case 1. Case 2 refers to sites with defects observed only in AFM, indicating that the docking site functioned properly during DNA-PAINT but may have incurred damage prior to or during AFM imaging. Case 3 refers to sites with defects observed only in DNA-PAINT, speculated to result from incorporated strands with truncated docking sites, single site defects, or inaccessible docking sites. Case 4 refers to sites with defects observed in both AFM and DNA-PAINT and distinguishes unincorporated docking sites from other types of defects. Of particular interest are Cases 3 and 4, which correspond to incorporated but inactive strands and unincorporated strands, respectively. To supplement the results of correlative defect metrology, which was limited to sample sizes of a few hundred structures, full area DNA-PAINT images were classified and counted using a convolution neural network (SI B4 and Figures S13 and 14). This enabled analysis of several thousand structures per sample and provided a statistically accurate measure of docking site availability for each sample.

The results of defect metrology are summarized in Figure 4, and details on the results of individual samples are provided in SI Figures S15-S17. Incremental improvements in docking site availability were observed for the duplexed-PAGE sample  $(86 \pm 2\%, n = 344)$  over the control sample  $(81 \pm 3\%, n =$ 319). PAGE filtration alone (81  $\pm$  2%, n = 377) did not increase docking site availability over the control for structures quantified by correlative defect metrology, though automated classification of full DNA-PAINT images did reveal a modest improvement upon strand filtration, with unfiltered, PAGE, and duplexed-PAGE samples having docking site availabilities of 82.2  $\pm$  0.7%, 84.3  $\pm$  0.2%, and 86.0  $\pm$  0.1%, respectively (n > 4000 for all samples). The most intriguing results arose from the correlated image analysis. We found that the probability of strand incorporation was significantly higher than has been reported previously for all samples, with 97  $\pm$  3% of docking site strands incorporated in the control and 98  $\pm$  1% incorporated in the filtered samples. Approximately 84  $\pm$ 19% of unavailable sites were found to be incorporated in the control sample and 88 ± 6% were incorporated in samples containing PAGE and duplexed-PAGE filtered docking sites.

The results of correlative defect analysis suggest that inactive/inaccessible docking sites, rather than unincorporated strands, play a significant role in limiting the addressability of DNA origami. We previously speculated that local defects in the docking sites might account for the population of inactive sites, yet only incremental gains were observed with staple strand filtration intended to remove the defective strands, suggesting the presence of unidentified factors limiting docking site availability. The results of correlative defect metrology ruled out unincorporated strands as a significant source of defects for the sites of interest in the DNA origami cross-tile, thus we limited our characterization to DNA-PAINT for further investigations. We performed additional experiments on origami possessing docking sites with a base substitution at the terminal end of the docking site (SI Figures S18-S20), though it was found that such n-1 defects, which shorten the docking site domain by 1 nt, had negligible effects on docking

site availability in DNA-PAINT (Figure 5, SI Figure S21).

Based on recent reports, 56,57 we speculated that docking sites may become deactivated during sample processing or imaging by exposure to UV or by photooxidation. To explore the impact of photooxidation and UV damage on site availability, several additional experiments were performed on

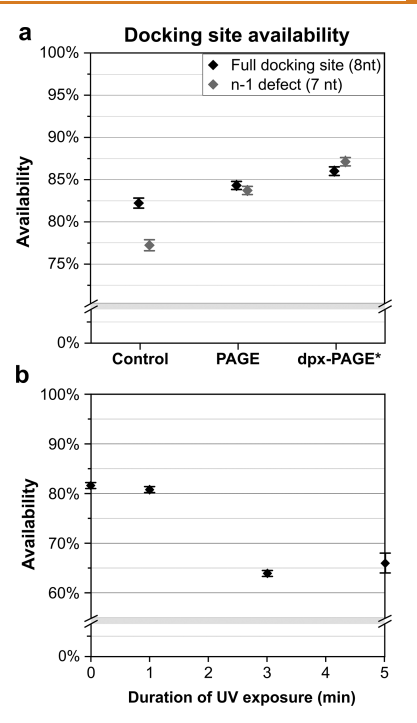


Figure 5. Effects of n-1 defects and UV irradiation on docking site availability. (a) Plot of the docking site availability for six sets of cross-tiles containing either full docking sites (8 nt, black) or docking sites with an n-1 defect (7 nt, gray) which were unfiltered (Control), PAGE-filtered (PAGE), or duplexed PAGE-filtered (dpx-PAGE) prior to origami synthesis. The introduction of n-1 defects did not significantly affect docking site availability for filtered samples. \*7 nt docking sites were filtered using a variation of the dpx-PAGE technique, detailed in SI A16 and Figure \$20. (b) Plot of the docking site availability for cross-tiles exposed to 305 nm UV on a benchtop UV transilluminator for 0, 1, 3, or 5 min. All availabilities were determined from automated classification of a minimum of 4000 cross-tiles per sample.

samples with intentionally induced defects. Defects caused by UV exposure were introduced by varying the duration of origami exposure to 305 nm UV light in an agarose gel prior to extraction, and the effects of photooxidation during optical imaging were targeted by the inclusion of an oxygen-scavenger during DNA-PAINT (PCA/PCD and Trolox, SI A17).<sup>62</sup> All experiments on UV exposure included an oxygen-scavenger and were performed in a sealed microchannel. It is also worth noting that new docking site strands were purchased for these experiments due to depleted stock solutions. As expected, increasing the duration of UV exposure resulted in a reduction of docking site availability, decreasing from 81.6  $\pm$  0.6% without UV exposure to 80.8%  $\pm$  0.2% with 1 min exposure and down to 63.9%  $\pm$  0.2% for 3 min (Figure 5, SI Figures S22 and 23).

Correlative defect metrology was performed on samples with and without oxygen-scavengers in solution to determine whether photooxidation causes structural defects that can be detected by AFM. As photooxidation requires the excitation of a fluorophore, we speculated that such defects would manifest on sites resolved in DNA-PAINT as defects in AFM (Case 2). Interestingly, the control sample, prepared without oxygen-scavengers, outperformed the oxygen-scavengers sample with

 $85.2 \pm 0.8\%$  docking site availability and  $99 \pm 1\%$  strand incorporation, whereas the oxygen-scavengers sample had  $80.8 \pm 0.2\%$  docking site availability and  $95.7 \pm 0.2\%$  strand incorporation (SI Figures S24 and 25). There was also no reduction of sites classified as Case 2 with inclusion of the oxygen-scavengers, suggesting that photooxidation was not a significant source of structural defects in our experiments. Despite these results, we could not conclusively rule out the effects of photooxidation, as inclusion of an oxygen-scavenger necessitated use of varied buffer conditions during imaging that likely affected the stability of DNA origami on the surface.

#### **CONCLUSION**

In this work, we demonstrated a methodology for correlative DNA-PAINT/AFM microscopy of DNA nanostructures which enables the acquisition of high-resolution optical and topographic images without compromising image quality. To overcome substrate compatibility challenges often encountered in correlative microscopies, we identified a simple yet effective method to prepare glass substrates for selective immobilization of DNA origami but not imager strands. We achieved high quality correlation between structures in DNA-PAINT and AFM images, observing an average spatial deviation that could be fully accounted for by the single molecule localization uncertainty of the super-resolution image. Investigations of unresolved docking sites showed little correlation to structural defects observed with AFM, revealing that most site defects occur on strands that are present on the structure. We employed staple strand purification methods, oxygen scavenging, and limited UV exposure to improve the addressability of docking sites, however the results do not identify all possible causes and more work is needed to elucidate the mechanisms that limit site availability on DNA nanostructures. Lastly, we speculate that there is significant room for progress in the design of addressable sites that circumvent the effects of strand defects without the need to eliminate such defects entirely. A greater understanding of defect mechanisms will help to inform improved design principles and accelerate this progress, thereby increasing the yield and fidelity of DNA-based nanostructures.

## MATERIALS AND METHODS

Materials. Unmodified DNA oligonucleotides (SI Tables S1-S3) were purchased from Integrated DNA technologies. Cy3b modified DNA oligomers (SI Table S4) were purchased from Bio-Synthesis. M13mp18 scaffold was purchased from Bayou Biolabs (cat: P-107). Agarose (cat: R0492), 10× Tris-borate EDTA (TBE, 890 mM Tris, 890 mM boric acid, 20 mM EDTA, cat: FERB52), 100× Tris-EDTA (TE, cat: BP1338-1), magnesium chloride (MgCl<sub>2</sub>) hexahydrate (cat: AC197530010), nickel(II) chloride (NiCl<sub>2</sub>) hexahydrate (cat: 50-901-14780), and SYBR gold nucleic acid gel stain (cat: S11494) were purchased from Fisher Scientific. 20% Ficoll solution (cat: F5415-50 ML) was purchased from Sigma-Aldrich. 30% Acrylamide/ Bis solution 29:1 (cat: 1610156) was purchased from Bio-Rad. Tetramethylethylenediamine (TEMED, cat: BP150-100) and ammonium persulfate (APS, cat: AC327081000) were purchased from Fisher Scientific. Cover glass mounts were designed and machined in house. Gold Seal #1 cover glass (cat: 260341) were purchased from Ted Pella. 150 nm silane polymer-coated spherical AuNPs (part: E11-150-Silane-2.5) were custom ordered from Nanopartz. Alconox Liquinox (cat: NC9906065) and methanol (cat: AA19393K2) were purchased from Fisher Scientific. Type-F immersion oil (cat: MOIL-30) was purchased from ThorLabs. Bruker FastScan D AFM tips (cat: FASTSCAN-D) were purchased from Bruker. Fluoroelastomer Xprofile o-rings (cat: 6450K126) and 2-56 flathead screws (cat:

92210A076) were purchased from Grainger. Protocatechuic acid (PCA, cat: AAB2401636), protocatechuate-3,4-dioxygenase (PCD, cat: ICN15197525), and 6-hydroxy-2,5,7,8-tetramethylchroman-2-carboxylic acid (Trolox, cat: AC218940250) were purchased from Fisher Scientific. Purified and deionized (DI) water was acquired from a Barnstead Nanopure water purification system from Thermo Scientific.

DNA Origami Synthesis. Cross-shaped DNA origami tiles (SI Figure S1, Tables S1-S3) were prepared with 10 nM M13mp18 scaffold, 50 nM unmodified oligomers, and 500 nM docking oligomers in 0.5× TBE buffer with 12.5 mM MgCl<sub>2</sub>. Thermal annealing was performed in an Eppendorf Mastercycler Nexus Gradient thermal cycler using a previously reported recipe, provided in SI Table S5. After annealing, cross-tiles were stained with 0.1× SYBR Gold and mixed with loading buffer (0.5× TBE, 20% Ficoll solution in water) at 5:1 origami solution to loading buffer. DNA origami were filtered by agarose gel electrophoresis (0.8% agarose, 0.5× TBE, 8 mM MgCl<sub>2</sub>) at 7 V/cm for 90 min uncooled. Filtered DNA origami structure bands were identified under 305 nm UV light illumination and cut from the gel, and origami were extracted from the gel by compressing the agarose between glass slides. DNA origami concentrations were determined using a Thermo Scientific NanoDrop One microvolume UV-vis spectrophotometer.

Cover Glass Substrate Preparation. Prior to cleaning, No. 1 cover glass (22 mm × 22 mm) were inscribed in the upper corner of each slide for orientation, and cross-marks were inscribed at the center of each slide for registration during imaging. Cover glass were first cleaned by ultrasonic agitation (sonication) in 0.1% Liquinox surfactant, then sonicated in deionized water to remove remaining surfactant. Cover glass were dried by centrifugation and stored at 40 °C for at least 30 min. After cleaning, 50 µL of 200 fM silanized AuNPs (150 nm diameter) in methanol were deposited on the cover glass and incubated for 10 min, adding methanol occasionally to prevent drying. Cover glass were rinsed with methanol, submerged several times in DI water, and dried by slowly withdrawing the cover glass from the water bath. Excess water was wicked from the surface with a lab wipe, then the cover glass were placed in the incubation chamber at 40 °C and stored until use. To prepare cover glass for sample deposition, substrates were placed with the AuNP-functionalized surface face up in a glow discharge vacuum chamber (SI Figure S2a), and the chamber was pumped down to 2 Torr. Valves into the chamber were closed to maintain pressure statically, then glow discharge was activated for 75 s. The chamber was then vented slowly, and cover glass were assembled into the reusable fluidic chamber or a sealed microchannel for DNA origami deposition.

**DNA Origami Immobilization.** For correlative DNA-PAINT/ AFM imaging of DNA origami cross-tiles, 0.1 nM origami in 200  $\mu$ L working buffer (0.5× TBE and 18 mM MgCl<sub>2</sub>, pH 8.3) were deposited on the surface of cover glass immediately after glow discharge and incubated for 30 min. Excess cross-tiles were rinsed from the surface with buffer, and samples were hydrated with 400  $\mu$ L working buffer until imaging.

Optical Imaging. Optical imaging was performed on a modified Nikon Eclipse TiU microscope equipped with a Nikon Total Internal Reflection Fluorescence (TIRF) illuminator and CFI Apo TIRF 100× NA 1.49 objective. A 561 nm Coherent Sapphire laser was used for excitation with a 0.5× stop down (approximately 8 mW TIRF illumination), and spectral filtration was performed with a Chroma TRF49909 ET-561 nm filter set. An additional 1.5× magnification was used to achieve a total magnification of 150× and pixel size of 107 nm. Images were acquired using a Princeton Instruments ProEM EMCCD camera controlled by the imaging software LightField, set to 100× EM gain with low analog gain and 150 ms/frame (6.67 Hz) acquisition. The area captured within each image is  $55 \times 55 \,\mu\text{m}^2$  with a  $512 \times 512$  px sensor ROI. Focal drift was corrected in real time with an optical setup and feedback loop controlling a Mad City Laboratories (MCL) Nano-Drive piezo stage. Precise stage movements for registration were performed with an MCL Micro-Drive stepper motor stage. Reusable cover glass mounts were designed and machined from aluminum in house to enable deconstruction of the

fluidic chamber without damaging the cover glass substrate (SI Figure S2b). Cover glass was held in place by compression against an O-ring and could be easily removed from the mount after TIRF imaging. For DNA-PAINT image acquisition, 400  $\mu$ L of imaging solution (3 nM Cy3-labeled imager strands in working buffer) was added to the fluidic chamber. 24 000 frames were acquired with 150 ms/frame for a total of 1 h acquisition. After imaging, the fluidic chamber was rinsed twice with 400  $\mu$ L of filtered working buffer, then the sample was transferred for AFM imaging.

AFM Imaging. AFM images were acquired in fluid on a Bruker Dimension FastScan with fluid tapping mode and Bruker FastScan D AFM tips. The fluidic chamber was deconstructed to provide access to the substrate, and the cover glass was placed on a silicone pad and mounted on the AFM stage. The sample was rinsed with 300 µL of filtered working buffer, then 300  $\mu$ L of filtered working buffer with 1 mM NiCl<sub>2</sub> was deposited on the surface and incubated for 5 min. For imaging, 300  $\mu$ L of filtered working buffer was deposited on the surface. The AFM tip was aligned over the center of the registration mark, then steps of 70  $\mu$ m were performed in the X and Y axes to relocate the correct ROI, accounting for any changes in the orientation of the substrate. The sample was then engaged, and high-resolution AFM images (1 nm<sup>2</sup>/px and 1 or 2  $\mu$ m per side) were captured. 50  $\mu$ L of DI water was added to the sample every 30 min to counteract evaporation. Large area AFM images (5  $\mu$ m, 10  $\mu$ m, and/ or 20  $\mu$ m per side, 2000 × 2000 px) were then acquired, centered on the original ROI.

## **ASSOCIATED CONTENT**

## **Supporting Information**

The Supporting Information is available free of charge at https://pubs.acs.org/doi/10.1021/acsnano.1c01976.

Optical and AFM setups, substrate preparation, and imaging protocols, DNA origami synthesis and filtration, image postprocessing and alignment, single-molecule binding kinetics and image acquisition, identification of defects in AFM, image correlation, results of correlative defect metrology, strand filtration methods, and list of staple strands for the DNA origami cross-tile (PDF)

# **AUTHOR INFORMATION**

# **Corresponding Authors**

Christopher M. Green — Center for Bio/Molecular Science and Engineering, U.S. Naval Research Laboratory Code 6900, Washington, D.C. 20375, United States; National Research Council, Washington, D.C. 20001, United States; orcid.org/0000-0001-7848-7144;

Email: CMGreen011@gmail.com

Wan Kuang — Department of Electrical & Computer Engineering, Boise State University, Boise, Idaho 83725, United States; Email: WanKuang@boisestate.edu

# Authors

William L. Hughes – Micron School of Materials Science & Engineering, Boise State University, Boise, Idaho 83725, United States; orcid.org/0000-0003-0102-3573

Elton Graugnard — Micron School of Materials Science & Engineering, Boise State University, Boise, Idaho 83725, United States; Orcid.org/0000-0002-0497-9821

Complete contact information is available at: https://pubs.acs.org/10.1021/acsnano.1c01976

#### Notes

The authors declare no competing financial interest.

## **ACKNOWLEDGMENTS**

This work was jointly supported by the National Science Foundation (CMMI-1344915 and Award Number 1807809) the Semiconductor Research Corporation (Nucleic Acid Memory 2842.001), and the Idaho Global Entrepreneurial Mission. The authors thank the Boise State Surface Science Laboratory for support of the atomic force microscope.

#### **REFERENCES**

- (1) Li, X.; Yang, X.; Qi, J.; Seeman, N. C. Antiparallel DNA Double Crossover Molecules as Components for Nanoconstruction. *J. Am. Chem. Soc.* **1996**, *118*, 6131–6140.
- (2) Mirkin, C. A.; Letsinger, R. L.; Mucic, R. C.; Storhoff, J. J. A DNA-Based Method for Rationally Assembling Nanoparticles into Macroscopic Materials. *Nature* **1996**, 382, 607–609.
- (3) Seeman, N. C. Nucleic Acid Junctions and Lattices. J. Theor. Biol. 1982, 99, 237–247.
- (4) Seeman, N. C. DNA Nanotechnology: Novel DNA Constructions. Annu. Rev. Biophys. Biomol. Struct. 1998, 27, 225-248.
- (5) Rothemund, P. W. Folding DNA to Create Nanoscale Shapes and Patterns. *Nature* **2006**, 440, 297–302.
- (6) Kuzyk, A.; Jungmann, R.; Acuna, G. P.; Liu, N. DNA Origami Route for Nanophotonics. ACS Photonics 2018, 5, 1151–1163.
- (7) Pilo-Pais, M.; Acuna, G. P.; Tinnefeld, P.; Liedl, T. Sculpting Light by Arranging Optical Components with DNA Nanostructures. *MRS Bull.* **2017**, 42, 936–942.
- (8) Bui, H.; Onodera, C.; Kidwell, C.; Tan, Y.; Graugnard, E.; Kuang, W.; Lee, J.; Knowlton, W. B.; Yurke, B.; Hughes, W. L. Programmable Periodicity of Quantum Dot Arrays with DNA Origami Nanotubes. *Nano Lett.* **2010**, *10*, 3367–3372.
- (9) Schreiber, R.; Do, J.; Roller, E. M.; Zhang, T.; Schuller, V. J.; Nickels, P. C.; Feldmann, J.; Liedl, T. Hierarchical Assembly of Metal Nanoparticles, Quantum Dots and Organic Dyes Using DNA Origami Scaffolds. *Nat. Nanotechnol.* **2014**, *9*, 74–78.
- (10) Ko, S. H.; Gallatin, G. M.; Liddle, J. A. Nanomanufacturing with DNA Origami: Factors Affecting the Kinetics and Yield of Quantum Dot Binding. *Adv. Funct. Mater.* **2012**, 22, 1015–1023.
- (11) Shen, B.; Kostiainen, M. A.; Linko, V. DNA Origami Nanophotonics and Plasmonics at Interfaces. *Langmuir* **2018**, *34*, 14911–14920.
- (12) Gur, F. N.; Schwarz, F. W.; Ye, J.; Diez, S.; Schmidt, T. L. Toward Self-Assembled Plasmonic Devices: High-Yield Arrangement of Gold Nanoparticles on DNA Origami Templates. *ACS Nano* **2016**, 10, 5374—5382.
- (13) Klein, W. P.; Schmidt, C. N.; Rapp, B.; Takabayashi, S.; Knowlton, W. B.; Lee, J.; Yurke, B.; Hughes, W. L.; Graugnard, E.; Kuang, W. Multiscaffold DNA Origami Nanoparticle Waveguides. *Nano Lett.* **2013**, *13*, 3850–3856.
- (14) Takabayashi, S.; Klein, W. P.; Onodera, C.; Rapp, B.; Flores-Estrada, J.; Lindau, E.; Snowball, L.; Sam, J. T.; Padilla, J. E.; Lee, J.; Knowlton, W. B.; Graugnard, E.; Yurke, B.; Kuang, W.; Hughes, W. L. High Precision and High Yield Fabrication of Dense Nanoparticle Arrays onto DNA Origami at Statistically Independent Binding Sites. *Nanoscale* 2014, 6, 13928–13938.
- (15) Simmel, F. C.; Yurke, B.; Singh, H. R. Principles and Applications of Nucleic Acid Strand Displacement Reactions. *Chem. Rev.* **2019**, *119*, 6326–6369.
- (16) Chandrasekaran, A. R. DNA Origami and Biotechnology Applications: A Perspective. *J. Chem. Technol. Biotechnol.* **2016**, 91, 843–846.
- (17) Voigt, N. V.; Torring, T.; Rotaru, A.; Jacobsen, M. F.; Ravnsbaek, J. B.; Subramani, R.; Mamdouh, W.; Kjems, J.; Mokhir, A.; Besenbacher, F.; Gothelf, K. V. Single-Molecule Chemical Reactions on DNA Origami. *Nat. Nanotechnol.* **2010**, *5*, 200–203.
- (18) Chatterjee, G.; Dalchau, N.; Muscat, R. A.; Phillips, A.; Seelig, G. A Spatially Localized Architecture for Fast and Modular DNA Computing. *Nat. Nanotechnol.* **2017**, *12*, 920–927.

- (19) Bui, H.; Shah, S.; Mokhtar, R.; Song, T.; Garg, S.; Reif, J. Localized DNA Hybridization Chain Reactions on DNA Origami. *ACS Nano* **2018**, *12*, 1146–1155.
- (20) Chao, J.; Zhu, D.; Zhang, Y.; Wang, L.; Fan, C. DNA Nanotechnology-Enabled Biosensors. *Biosens. Bioelectron.* **2016**, *76*, 68–79
- (21) Pei, H.; Zuo, X.; Pan, D.; Shi, J.; Huang, Q.; Fan, C. Scaffolded Biosensors with Designed DNA Nanostructures. *NPG Asia Mater.* **2013**, *5*, No. e51.
- (22) Thubagere, A. J.; Li, W.; Johnson, R. F.; Chen, Z.; Doroudi, S.; Lee, Y. L.; Izatt, G.; Wittman, S.; Srinivas, N.; Woods, D.; Winfree, E.; Qian, L. A Cargo-Sorting DNA Robot. *Science* **2017**, 357, 1–11.
- (23) Gothelf, K. V. Chemical Modifications and Reactions in DNA Nanostructures. MRS Bull. 2017, 42, 897–903.
- (24) Kotani, S.; Hughes, W. L. Multi-Arm Junctions for Dynamic DNA Nanotechnology. J. Am. Chem. Soc. 2017, 139, 6363–6368.
- (25) Galatsis, K.; Wang, K. L.; Ozkan, M.; Ozkan, C. S.; Huang, Y.; Chang, J. P.; Monbouquette, H. G.; Chen, Y.; Nealey, P.; Botros, Y. Patterning and Templating for Nanoelectronics. *Adv. Mater.* **2010**, 22, 769–778.
- (26) Gao, B.; Sarveswaran, K.; Bernstein, G. H.; Lieberman, M. Guided Deposition of Individual DNA Nanostructures on Silicon Substrates. *Langmuir* **2010**, *26*, 12680–12683.
- (27) Gates, E. P.; Dearden, A. M.; Woolley, A. T. DNA-Templated Lithography and Nanofabrication for the Fabrication of Nanoscale Electronic Circuitry. *Crit. Rev. Anal. Chem.* **2014**, *44*, 354–370.
- (28) Takabayashi, S.; Kotani, S.; Flores-Estrada, J.; Spears, E.; Padilla, J. E.; Godwin, L. C.; Graugnard, E.; Kuang, W.; Sills, S.; Hughes, W. L. Boron-Implanted Silicon Substrates for Physical Adsorption of DNA Origami. *Int. J. Mol. Sci.* **2018**, *19*, 1–11.
- (29) Liddle, J. A.; Gallatin, G. M. Lithography, Metrology And Nanomanufacturing. *Nanoscale* **2011**, *3*, 2679–2688.
- (30) Liddle, J. A.; Gallatin, G. M. Nanomanufacturing: A Perspective. ACS Nano 2016, 10, 2995–3014.
- (31) Grossi, G.; Jaekel, A.; Andersen, E. S.; Saccà, B. Enzyme-Functionalized DNA Nanostructures as Tools for Organizing and Controlling Enzymatic Reactions. MRS Bull. 2017, 42, 920–924.
- (32) Samanta, A.; Medintz, I. L. Nanoparticles and DNA A Powerful and Growing Functional Combination in Bionanotechnology. *Nanoscale* **2016**, *8*, 9037–9095.
- (33) Castro, C. E.; Kilchherr, F.; Kim, D. N.; Shiao, E. L.; Wauer, T.; Wortmann, P.; Bathe, M.; Dietz, H. A Primer to Scaffolded DNA Origami. *Nat. Methods* **2011**, *8*, 221–229.
- (34) Douglas, S. M.; Marblestone, A. H.; Teerapittayanon, S.; Vazquez, A.; Church, G. M.; Shih, W. M. Rapid Prototyping of 3D DNA-Origami Shapes with Cadnano. *Nucleic Acids Res.* **2009**, *37*, 5001–5006.
- (35) Dunn, K. E.; Dannenberg, F.; Ouldridge, T. E.; Kwiatkowska, M.; Turberfield, A. J.; Bath, J. Guiding the Folding Pathway of DNA Origami. *Nature* **2015**, *525*, 82–86.
- (36) Kosinski, R.; Mukhortava, A.; Pfeifer, W.; Candelli, A.; Rauch, P.; Sacca, B. Sites of High Local Frustration in DNA Origami. *Nat. Commun.* **2019**, *10*, 1–12.
- (37) Song, J.; Arbona, J. M.; Zhang, Z.; Liu, L.; Xie, E.; Elezgaray, J.; Aime, J. P.; Gothelf, K. V.; Besenbacher, F.; Dong, M. Direct Visualization of Transient Thermal Response of a DNA Origami. *J. Am. Chem. Soc.* **2012**, *134*, 9844–9847.
- (38) Stahl, E.; Martin, T. G.; Praetorius, F.; Dietz, H. Facile and Scalable Preparation of Pure and Dense DNA Origami Solutions. *Angew. Chem., Int. Ed.* **2014**, 53, 12735–12740.
- (39) Strauss, M. T.; Schueder, F.; Haas, D.; Nickels, P. C.; Jungmann, R. Quantifying Absolute Addressability in DNA Origami with Molecular Resolution. *Nat. Commun.* **2018**, *9*, 1–7.
- (40) Tikhomirov, G.; Petersen, P.; Qian, L. Fractal Assembly of Micrometre-Scale DNA Origami Arrays with Arbitrary Patterns. *Nature* **2017**, 552, 67–71.
- (41) Zadegan, R. M.; Norton, M. L. Structural DNA Nanotechnology: From Design to Applications. *Int. J. Mol. Sci.* **2012**, *13*, 7149–7162.

- (42) Pan, K.; Bricker, W. P.; Ratanalert, S.; Bathe, M. Structure and Conformational Dynamics of Scaffolded DNA Origami Nanoparticles. *Nucleic Acids Res.* **2017**, *45*, 6284–6298.
- (43) Kozyra, J.; Ceccarelli, A.; Torelli, E.; Lopiccolo, A.; Gu, J. Y.; Fellermann, H.; Stimming, U.; Krasnogor, N. Designing Uniquely Addressable Bio-Orthogonal Synthetic Scaffolds for DNA and RNA Origami. ACS Synth. Biol. 2017, 6, 1140–1149.
- (44) Veneziano, R.; Ratanalert, S.; Zhang, K.; Zhang, F.; Yan, H.; Chiu, W.; Bathe, M. Designer Nanoscale DNA Assemblies Programmed from the Top Down. *Science* **2016**, 352, 1534–1543.
- (45) Mathur, D.; Medintz, I. L. Analyzing DNA Nanotechnology: A Call to Arms for the Analytical Chemistry Community. *Anal. Chem.* **2017**, 89, 2646–2663.
- (46) Mathur, D.; Medintz, I. L. The Growing Development of DNA Nanostructures for Potential Healthcare-Related Applications. *Adv. Healthcare Mater.* **2019**, *8*, No. e1801546.
- (47) Green, C. M.; Mathur, D.; Medintz, I. L. Understanding the Fate of DNA Nanostructures inside the Cell. *J. Mater. Chem. B* **2020**, *8*, 6170–6178.
- (48) Schnitzbauer, J.; Strauss, M. T.; Schlichthaerle, T.; Schueder, F.; Jungmann, R. Super-Resolution Microscopy with DNA-PAINT. *Nat. Protoc.* **2017**, *12*, 1198–1228.
- (49) Jungmann, R.; Steinhauer, C.; Scheible, M.; Kuzyk, A.; Tinnefeld, P.; Simmel, F. C. Single-Molecule Kinetics and Super-Resolution Microscopy by Fluorescence Imaging of Transient Binding on DNA Origami. *Nano Lett.* **2010**, *10*, 4756–4761.
- (50) Jungmann, R.; Avendano, M. S.; Woehrstein, J. B.; Dai, M.; Shih, W. M.; Yin, P. Multiplexed 3D Cellular Super-Resolution Imaging with DNA-PAINT and Exchange-PAINT. *Nat. Methods* **2014**, *11*, 313–318.
- (51) Jungmann, R.; Avendano, M. S.; Dai, M.; Woehrstein, J. B.; Agasti, S. S.; Feiger, Z.; Rodal, A.; Yin, P. Quantitative Super-Resolution Imaging with qPAINT. *Nat. Methods* **2016**, *13*, 439–442.
- (52) Graugnard, E.; Hughes, W. L.; Jungmann, R.; Kostiainen, M. A.; Linko, V. Nanometrology and Super-Resolution Imaging with DNA. MRS Bull. 2017. 42, 951–959.
- (53) Iinuma, R.; Ke, Y.; Jungmann, R.; Schlichthaerle, T.; Woehrstein, J. B.; Yin, P. Polyhedra Self-Assembled from DNA Tripods and Characterized with 3D DNA-PAINT. *Science* **2014**, 344, 65–69.
- (54) Green, C. M.; Schutt, K.; Morris, N.; Zadegan, R. M.; Hughes, W. L.; Kuang, W.; Graugnard, E. Metrology of DNA Arrays by Super-Resolution Microscopy. *Nanoscale* **2017**, *9*, 10205–10211.
- (55) Odermatt, P. D.; Shivanandan, A.; Deschout, H.; Jankele, R.; Nievergelt, A. P.; Feletti, L.; Davidson, M. W.; Radenovic, A.; Fantner, G. E. High-Resolution Correlative Microscopy: Bridging the Gap between Single Molecule Localization Microscopy and Atomic Force Microscopy. *Nano Lett.* **2015**, *15*, 4896–904.
- (56) Blumhardt, P.; Stein, J.; Mucksch, J.; Stehr, F.; Bauer, J.; Jungmann, R.; Schwille, P. Photo-Induced Depletion of Binding Sites in DNA-PAINT Microscopy. *Molecules* **2018**, 23, 1–27.
- (57) Kielar, C.; Xin, Y.; Xu, X.; Zhu, S.; Gorin, N.; Grundmeier, G.; Moser, C.; Smith, D. M.; Keller, A. Effect of Staple Age on DNA Origami Nanostructure Assembly and Stability. *Molecules* **2019**, 24, 1–12.
- (58) Hauser, M.; Wojcik, M.; Kim, D.; Mahmoudi, M.; Li, W.; Xu, K. Correlative Super-Resolution Microscopy: New Dimensions and New Opportunities. *Chem. Rev.* **2017**, *117*, 7428–7456.
- (59) Liu, W.; Zhong, H.; Wang, R.; Seeman, N. C. Crystalline Two-Dimensional DNA-Origami Arrays. *Angew. Chem., Int. Ed.* **2011**, *50*, 264–267.
- (60) Aghebat Rafat, A.; Pirzer, T.; Scheible, M. B.; Kostina, A.; Simmel, F. C. Surface-Assisted Large-Scale Ordering of DNA Origami Tiles. *Angew. Chem., Int. Ed.* **2014**, *53*, 7665–7668.
- (61) Dickinson, G. D.; Mortuza, G. M.; Clay, W.; Piantanida, L.; Green, C. M.; Watson, C.; Hayden, E. J.; Andersen, T.; Kuang, W.; Graugnard, E.; Zadegan, R.; Hughes, W. L. An Alternative Approach to Nucleic Acid Memory. *Nat. Commun.* **2021**, *12*, 2371.

(62) Swoboda, M.; Henig, J.; Cheng, H. M.; Brugger, D.; Haltrich, D.; Plumere, N.; Schlierf, M. Enzymatic Oxygen Scavenging for Photostability without pH Drop in Single-Molecule Experiments. *ACS Nano* **2012**, *6*, 6364–6369.